JOURNAL OF GEOPHYSICAL RESEARCH: OCEANS, VOL. 119, 1–11, doi:10.1002/2013JC009240, 2014

Modeling Antarctic tides in response to ice shelf thinning and retreat

S. H. R. Rosier,[1,2] J. A. M. Green,[1] J. D. Scourse,[1] and R. Winkelmann[3]

Received 17 July 2013; revised 13 November 2013; accepted 12 December 2013.

[1] Tides play an important role in ice sheet dynamics by modulating ice stream velocity, fracturing, and moving ice shelves and mixing water beneath them. Any changes in ice shelf extent or thickness will alter the tidal dynamics through modification of water column thickness and coastal topography but these will in turn feed back onto the overall ice shelf stability. Here, we show that removal or reduction in extent and/or thickness of the Ross and Ronne-Filchner ice shelves would have a significant impact on the tides around Antarctica. The Ronne-Filchner appears particularly vulnerable, with an increase in M_2 amplitude of over 0.5 m beneath much of the ice shelf potentially leading to tidally induced feedbacks on ice shelf/sheet dynamics. These results highlight the importance of understanding tidal feedbacks on ice shelves/streams due to their influence on ice sheet dynamics.

Citation: Rosier, S. H. R., J. A. M. Green, J. D. Scourse, and R. Winkelmann (2014), Modeling Antarctic tides in response to ice shelf thinning and retreat, *J. Geophys. Res. Oceans*, *119*, doi:10.1002/2013JC009240.

1. Introduction

[2] Recent research has highlighted the important role that tides play in modulating ice stream velocities [*Anandakrishnan et al*., 2003; *Aethalgeirsdottir et al*., 2008; *King et al*., 2010, 2011; *Gudmundsson*, 2011]. Ice shelves buttress adjacent ice streams, slowing the outflow of ice from the Antarctic continent; rapid acceleration in ice stream velocity can follow ice shelf disintegration [*Rignot et al*., 2004; *Bamber et al*., 2007; *Rott et al*., 2011]. An additional and relatively unexplored mechanism is the impact of tides on ice shelf stability through vertical displacement and fracturing. Tides induce sea-level changes at the grounding line to which ice streams are highly sensitive, with implications for iceberg calving rates and the inland flow of ice sheets [*Vieli and Nick*, 2011; *Conway et al*., 1999; *Schoof*, 2007; *Goldberg et al*., 2009]. Aside from mechanical effects, tides have been shown to play a significant role in vertical mixing beneath ice shelves, affecting basal melt rate distribution and magnitude with implications for overall mass balance and stability [*Makinson et al*., 2011; *Mueller et al*., 2012]. If an ice shelf is perturbed in such a way as to reduce its extent and/or thickness or the position of the grounding line this would in turn affect the tide by changing local water column thickness or the position of the coastline. Tides are also known to play a significant role in controlling the stick-slip motion of ice streams [*Bindschadler et al*., 2003; *Winberry et al*., 2009] and both elastic [*King et al*., 2011] and viscoelastic [*Gudmundsson*, 2011] models have shown the importance of tides in modulating ice stream velocities, not only near the grounding line but also far upstream. Changes in tidal amplitudes following ice shelf collapse may thus have far reaching consequences for the dynamics of the ice sheets and global sea level [*Hemming*, 2004; *Fluckiger et al*., 2006]. Ice shelf-tide feedbacks have also been invoked to explain major catastrophic ice sheet collapse in the past, such as Heinrich events [e.g., *Arbic et al*., 2004a, 2004b], but our understanding of these feedback mechanisms is limited. The numerical simulations presented here demonstrate that hypothetical reductions in the extent of the Ross or Ronne-Filchner ice shelves could significantly alter tides in these regions, with implications for ice stream velocity and ice shelf stability which could lead to both positive and negative feedback situations depending on location.

[3] Since the collapse of the Larsen B Ice Shelf in 2002 there has been a growing realization of the vulnerability of ice shelves in a warming environment [*Glasser and Scambos*, 2008]. Whilst current trends do not suggest that the Ross or Ronne-Filchner ice shelves are reducing in mass [*Shepherd et al*. 2010; *Pritchard et al*., 2012], recent work has shown potential mechanisms for reductions in thickness of the Ronne-Filchner [*Hellmer et al*., 2012], and other ice shelves are known to have collapsed in the past [Ó *Cofaigh*, 2011] indicating that the Larsen B collapse was not an isolated event. The mechanism by which changes in ice shelf/stream geometry could alter local tides was explored by *Griffiths and Peltier* [2009] for the polar regions during the Last Glacial Maximum (LGM). While the extent of the changes in ice topography were greater than those we are considering here, their results

[1]School of Ocean Sciences, College of Natural Sciences, Bangor University, Bangor, UK.
[2]British Antarctic Survey, Cambridge, UK.
[3]Potsdam Institute for Climate Impact Research, Potsdam, Germany.

Corresponding author: S. H R. Rosier, School of Ocean Sciences, Bangor University, Bangor LL59 5AB, UK. (s.rosier@bangor.ac.uk)

©2013. American Geophysical Union. All Rights Reserved.
2169-9275/14/10.1002/2013JC009240

highlight the potentially large shifts in tidal regime that may have occurred in the past and the potential sensitivity of Antarctic tides to changes in the position of the grounding line. The nonlinear interaction shown by *Gudmundsson* [2011] to exist between tides and ice streams suggests that a change in tidal amplitudes will modify mean ice stream flow. Due to tidal sensitivity to bathymetry and coastal topography, it is to be expected that removal of floating ice will significantly alter tides across the Antarctic region. Here, we investigate the response of Antarctic tides to hypothetical reduction or removal of the Ronne-Filchner and Ross ice shelves. This work may be considered a sensitivity study of the Antarctic tidal regime and aims to reveal any areas of particular vulnerability warranting further investigation.

2. Methods

2.1. Tidal Modeling

[4] The Oregon State University Tidal Inversion Software (OTIS) is used here to simulate the Antarctic tides in a domain spanning 60–90°S in latitude and the full globe in longitude (see Figure 1). It has been used and validated extensively to simulate past, present, and future tidal regimes at a variety of scales [e.g., *Egbert et al*., 2004; *Green*, 2010; *Pelling and Green* 2013; *Green and Huber*, 2013] The model solves the linearized rotating shallow water equations subject to tidal forcing only, i.e.,

$$\frac{\partial \mathbf{U}}{\partial t} + f \times \mathbf{U} = -gh\nabla(\eta - \eta_{SAL} - \eta_{EQ}) + F \quad (1)$$

$$\frac{\partial \eta}{\partial t} = -\nabla \cdot \mathbf{U} \quad (2)$$

where $\mathbf{U} = \mathbf{u}$h, $\mathbf{u}$ is the total velocity vector for all constituents, water depth is h, f is the Coriolis vector, η is tidal elevation, η_{SAL} is the self-attraction and loading elevation (taken from satellite altimetry data, and not changed between the simulations), η_{EQ} is the equilibrium tide, and $F = F_b + \mathbf{F}_w$ parameterizes energy losses due to bed friction (F_b) and tidal conversion ($\mathbf{F}_w$). The first of these terms use a standard quadratic drag law, $F_b = C_d \mathbf{U}_1 \mathbf{u}_1 / h$ ($C_d \sim 0.003$ is a drag coefficient) represents bed friction, whereas the conversion is parameterized by the scheme presented by *Zaron and Egbert* [2006; see *Green and Nycander*, 2013, for details]. The latter is quite crude but computationally efficient, and it allows for conversion poleward of critical latitudes. It must be noted, however, that the conversion is relatively weak in this domain and bed friction dominates the shelf seas under investigation here. Grid spacing is 1/12° in both longitude and latitude and simulations were undertaken for the M_2, S_2, K_1, and O_1 constituents, with M_4 being an additional part of the output (but not included in the forcing). Note, however, that we focus on M_2, K_1, and M_4 in this paper. The bathymetry is a composite of various data sets described by *Padman and Fricker* [2005], whereas the water column thickness under the ice shelves and the ice shelf thickness are from BEDMAP [*Lythe and Vaughan*, 2001]. Forcing at the open boundary at 60°S consisted of elevations from the inverse TPXO7.2 solution [see *Egbert and Erofeeva*, 2002, for the methodology and http://volkov.oce.orst.edu/tides/global.html for the data]. Although the changes in ice shelf configuration outlined in this paper would require considerable perturbation in climate which may lead to changes in sea level, the open boundary is in the deep ocean and therefore is assumed to be largely unaffected by these changes (this is supported by the simulations in *Green* [2010]). In order to further ensure the location of the open boundary did not affect results, several simulations were done at different latitudinal boundaries (62°S and 65°S) and results remained unchanged.

2.2. Dissipation

[5] The tidal dissipation, D, can be computed using the model output as the difference between the work done by the tide producing force (W) and the divergence of the barotropic energy flux ($\nabla \cdot \mathbf{P}$) [*Egbert and Ray*, 2001]:

$$D = W - \nabla \cdot \mathbf{P} \quad (3)$$

[6] W and $\mathbf{P}$ are defined as

$$W = g\rho\langle \mathbf{U} \cdot \nabla(\eta_{EQ} + \eta_{SAL}) \rangle \quad (4)$$

$$\mathbf{P} = g\rho\langle \mathbf{U}\eta \rangle \quad (5)$$

in which the angular brackets mark time averages and the small Earth tide has been neglected.

2.3. Ice Shelf Configuration

[7] Several representations of the floating ice shelves were implemented in the model to test the sensitivity of the tides around Antarctica to changes in ice sheet geometry. The control run used water column thickness from the databases and a doubled bed friction under the ice shelves to simulate the enhanced drag under the shelves [*MacAyeal*, 1984; *Padman et al*., 2002]. Where present, the floating ice shelf is treated as a purely passive object and elastic forces near the grounding line are not considered. Simulations of removal of the Ronne-Filchner and Ross ice shelves (henceforth denoted "No Ice") added the ice draft given by BEDMAP to water thickness beneath the shelf in order to provide a total water depth, h, under ice free conditions. Runs were also undertaken in which the ice shelf thickness was halved ("HT"), in which both the Ronne-Filchner and Ross ice-shelf extents were halved with no change to the remaining shelf thickness ("HE"), and in which both extents and thicknesses were halved ("HTE"). In HE runs, the extent was halved by removing the shelf beyond latitudinal lines, resulting in approximately half the original shelf area, and the areas of increased bed friction were also altered to reflect this configuration.

[8] A number of other runs with various combinations of ice thickness and enhanced drag under the ice were also undertaken to test the sensitivity of the model to parameter values. It was found that increasing the bed friction under ice by a factor of 20 and slightly reducing ice shelf thickness improved accuracy compared to the heavily assimilated CATS2008a model [*Padman and Fricker*, 2005; *Padman et al*., 2008], but it was decided that this minor improvement does not justify the alterations to the default parameterization of ice shelves within the model where bed friction is doubled beneath the ice shelf. The increased

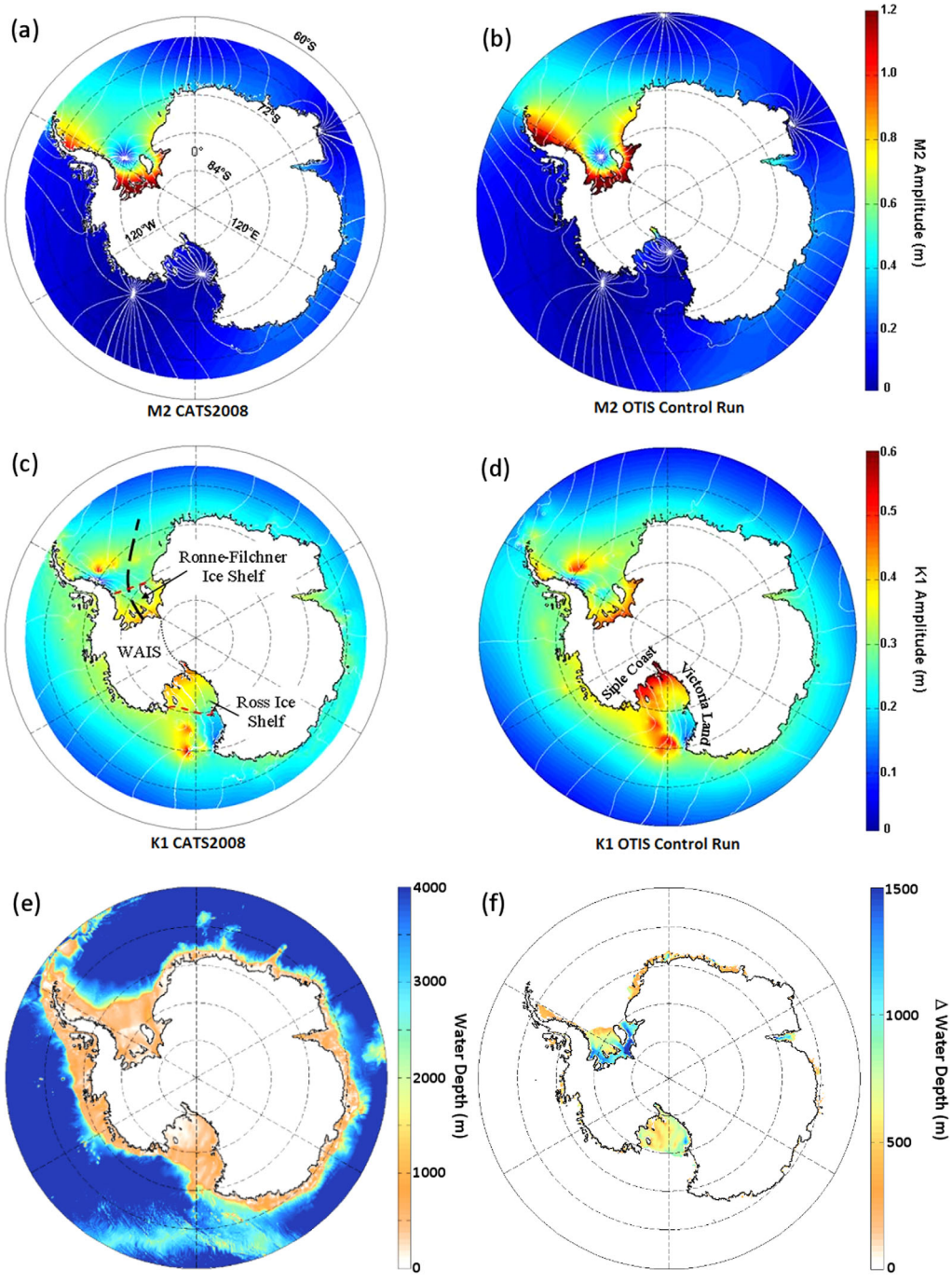

Figure 1. Tidal amplitudes (in meters) (left) from the CATS model output and (right) from the present OTIS simulation. (a and b) M_2 amplitudes, (c and d) K_1 amplitudes. The white contours mark relative phases with 20° separation. Dashed red lines in Figure 1c indicate the extent of the Ross and Ronne-Filchner Ice Shelves and the Antarctic Peninsula is the protruding region west of the Ronne Ice Shelf. The transect used for the response curve in Figure 4 is marked as a dashed line in Figure 1c. (e) Also shown is the bathymetry of the domain in meters and (f) the difference between the No Ice case and the control bathymetry.

accuracy resulting from increasing bed friction is not unexpected since the drag coefficient describes a roughness scale and the resolution of the bathymetry used—both at the bed and under the ice—is not fine enough to pick up the inherent roughness of the bed and particularly the underside of the ice.

3. Results

3.1. Control

[9] The control run results were compared to the CATS2008a model and shown to accurately reproduce the tidal amplitudes (Figure 1). We use the convention of *Arbic*

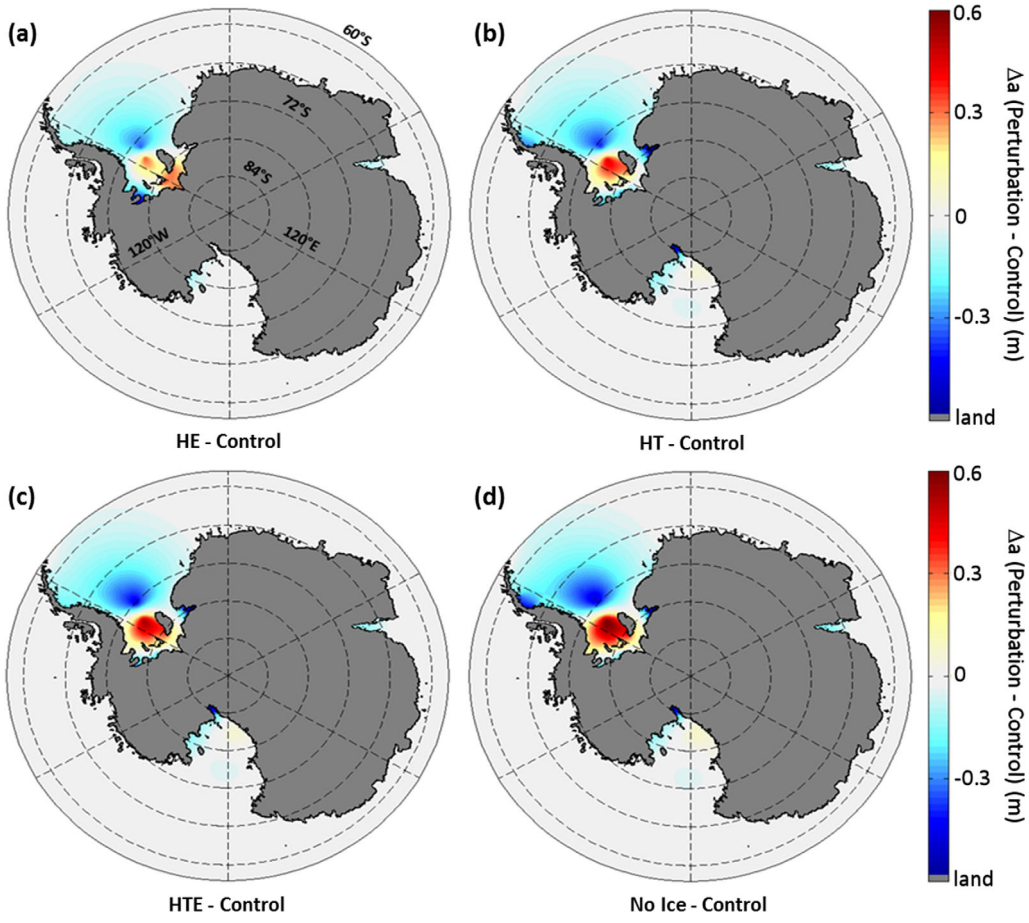

Figure 2. Change in M_2 tidal amplitude (compared to the control run where positive values indicate an increase in the perturbation run) resulting from removal of ice shelves for cases (a) HT, (b) HE, (c) HTE, and (d) No Ice. Note that M_2 amplitude changes under the Ross Ice Shelf are negligible but the M_2 tide in this region is very small in the control.

et al. [2004a, 2004b] to evaluate the agreement between the two models by calculating a root-mean-square difference (RMS):

$$\mathrm{RMS} = \sqrt{\frac{\langle \iint (\eta - \eta_{\mathrm{CATS}})^2 dA \rangle}{\iint dA}} \tag{6}$$

where η_{CATS} indicates the CATS2008a model output. From the CATS2008a model, we also compute a signal, S:

$$S = \sqrt{\frac{\langle \iint (\eta_{\mathrm{CATS}})^2 dA \rangle}{\iint dA}} \tag{7}$$

and finally the percentage of sea surface height variance (SSHV) captured by the model as

$$\mathrm{SSHV} = 100 \times [1 - (\mathrm{RMS}/\mathrm{S})^2]. \tag{8}$$

[10] There is good agreement between the two models, with a root-mean-square difference of 7.8 cm and 4.4 cm capturing 94% and 97% of the variance for M_2 and K_1, respectively, over the entire domain up to 62°S. Since a large part of the domain is in the deep ocean with small amplitude tides, values were also calculated for only shallow regions ($h < 1000$ m) which gave RMS values of 10.3 cm and 7.2 cm for M_2 and K_1, respectively. While these values are considerably larger the main trend in the results can still be considered robust as discussed below. The M_2 constituent has a reasonable amplitude in and around the Weddell Sea, whereas K_1 dominates the Ross Sea. Both the M_2 and K_1 amplitudes are generally overestimated in the control run (Figure 1) compared to the CATS2008a results. Of course, an assimilated model such as CATS2008a obtains better agreement with observations, but any perturbation experiments with an assimilated model are dubious at best. Because our model reproduces all the major tidal features in the region with reasonable accuracy we have confidence in our results.

3.2. Sensitivity Simulations

[11] The M_2 tide in the region is dominated by a large amphidromic point centered in the Weddell Sea which results in significantly lower tidal amplitudes beneath the center of the adjacent Ronne-Filchner Ice Shelf than would otherwise be the case. All perturbation runs show considerable amplification of the M_2 tide under the main body of the Ronne-Filchner ice shelf, with a stronger response when more of the ice shelves are removed (Figure 2).

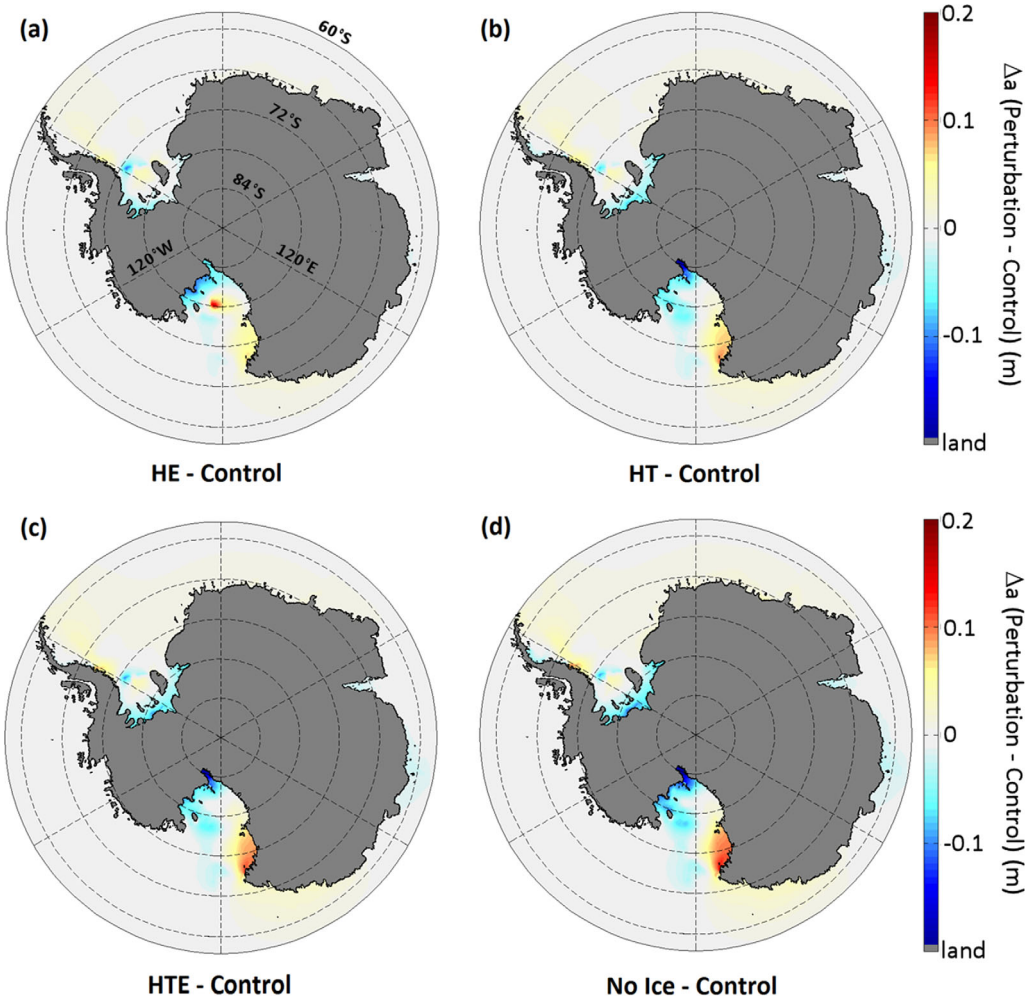

Figure 3. Change in K_1 tidal amplitude (compared to the control run where positive values indicate an increase in the perturbation run) resulting from removal of ice shelves for cases (a) HT, (b) HE, (c) HTE, and (d) No Ice.

Halving the extent of the ice shelves (Figure 2a) is found to produce less amplification than halving the thickness (Figure 2b) and sets up an additional bimodal response between the Filchner and Ronne ice shelves. Further amplification arises in the HTE run (Figure 2c) and the No Ice run (Figure 2d) shows reduction in M_2 amplitude along the eastern side of the Antarctic Peninsula.

[12] Because the K_1 tidal signal is not dominated by one amphidromic system but rather contains several features, the removal of ice shelves results in a less clear effect than for the M_2 constituent (Figure 3). The K_1 amplitude under the western Ross Ice Shelf is decreased by approximately 10 cm (17%) in all perturbation scenarios, and removing more ice increases the extent of the affected area. An additional response to the reduction of ice shelves is an increase in amplitude along the Victoria Land coastline, close to the ice front. In contrast, the tides in the Ronne-Filchner embayment show some decrease in K_1 amplitude along the grounding line once most of the ice has been removed. Overall, the changes in the K_1 constituent are of a much lower magnitude than the M_2 tide and whereas the largest effects on M_2 tend to be found centered under the Ronne Ice Shelf, K_1 effects tend to be most prominent closer to the coast.

[13] To further highlight the response, a transect of the M_2 tidal amplitude for the different simulations was plotted through the Ronne Ice Shelf (Figure 4a) along with the difference in perturbation amplitudes to the control (Figure 4b). Maximum amplification in the Weddell Sea is found with complete removal of the ice shelves at 77.5°S, with the M_2 amplitude more than doubling in this region. The M_2 amphidromic point moves away from the ice front in all the perturbation runs, not only due to the retreat of ice but also as a response to the changing water column thickness. Overall, the transect reveals M_2 amplification under the bulk of the Ronne Ice Shelf with amplitude under the center more than doubling.

[14] Tidal dissipation for the HT, HTE, and No Ice sensitivity simulations are compared to dissipation from equations (3)–(5) from the control run for the M_2 (Figure 5) and K_1 (Figure 6) tidal constituents. The dissipation estimates were split into total (i.e., for the whole domain), deep (i.e., the energy losses in water where $h > 1000$ m), and shallow (i.e., in water where $h < 1000$ m). Note that shallow and

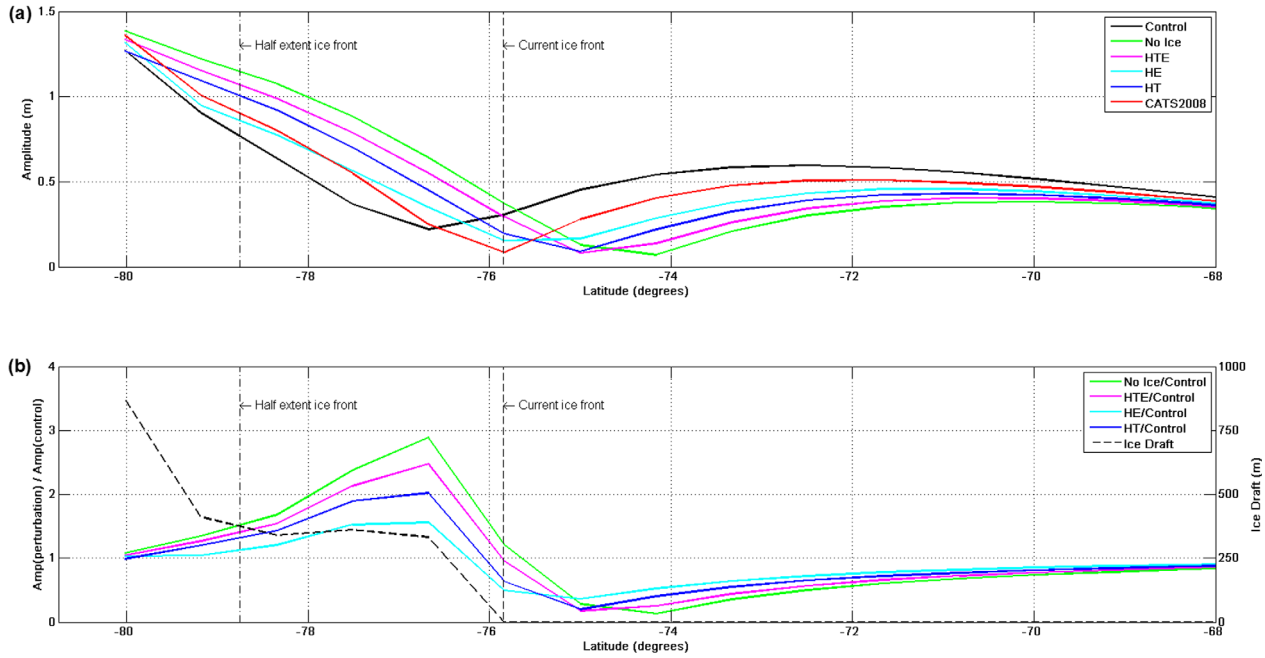

Figure 4. Response curve of M_2 amplitudes across transects (marked in Figure 1c) of the Ronne Ice Shelf to changes in ice cover. Note the location of the ice fronts for the present and HTE runs (dashed red lines).

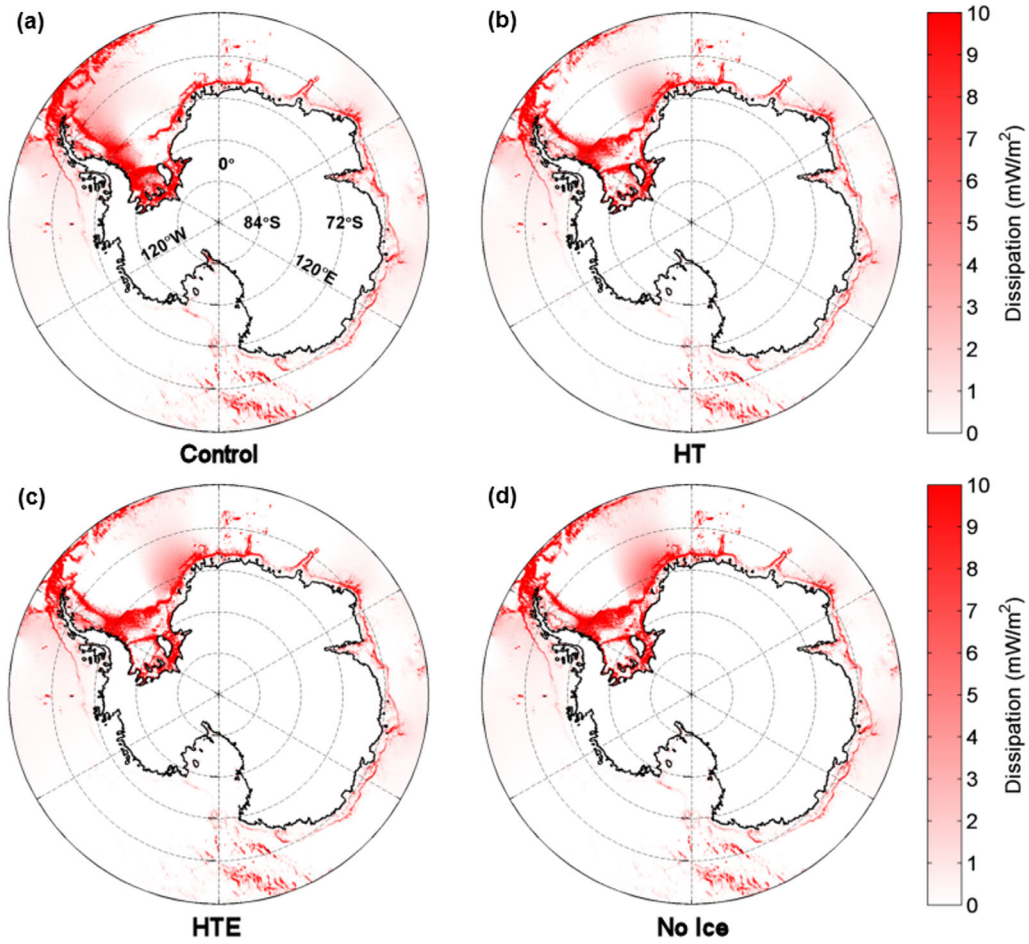

Figure 5. M_2 tidal dissipation for (a) the control run and the (b) HT, (c) HTE, and (d) No Ice perturbation runs.

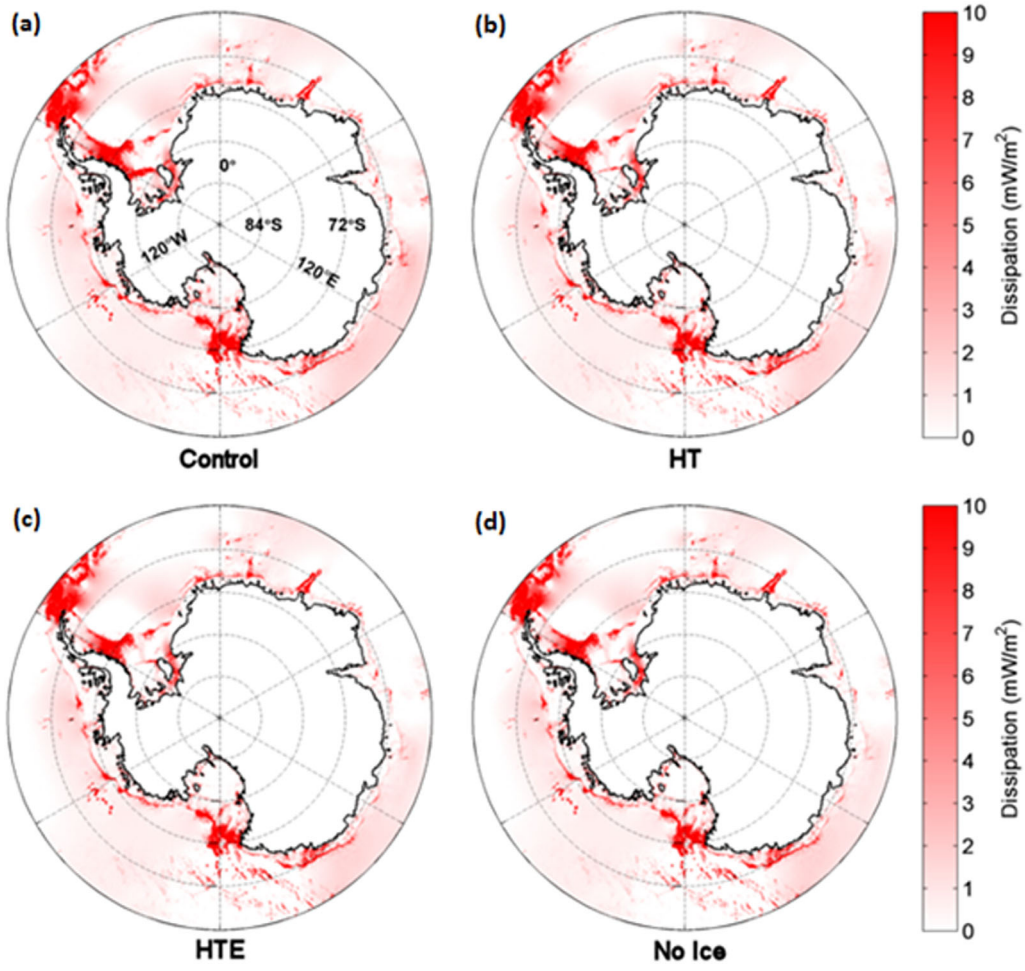

Figure 6. K_1 tidal dissipation for (a) the control run and the (b) HT, (c) HTE, and (d) No Ice perturbation runs.

deep regions were defined for each run separately to accommodate for changes in water depths. Changes in dissipation as a percent compared to the control are presented in Table 1.

[15] The M_2 tidal dissipation generally increases as the ice shelf is removed (Figure 5 and Table 1), with changes in total dissipation compared to the control of 42.2% for the No Ice run. Most of the change in dissipation occurs on the continental shelf, while the deep ocean dissipation initially decreased slightly for the HT run and increased for the HTE and No Ice runs. In contrast to this, K_1 dissipation decreases by 18.6% for the No Ice sensitivity run. Once again the change in shelf dissipation accounts for the majority of these changes and deep sea dissipation is only slightly reduced in all the runs.

4. PISM-PIK Simulations

4.1. Background

[16] As an extension to the sensitivity scenarios outlined above, tidal runs were performed for an Antarctic bathymetry derived from projections of ice extent by the Potsdam Parallel Ice Sheet Model (PISM-PIK) [*Martin et al*., 2011; *Winkelmann et al*., 2011, 2012] up to the year 2500. The PISM-PIK results were produced by forcing from the Extended Concentration Pathways (ECP) 8.5 climate scenario, in which greenhouse gas emissions continue to rise until the year 2250 at which point they begin to decline [*Meinshausen et al*., 2011]. Results from the PISM-PIK run were provided as anomalies in ice thickness and a shelf mask, in 100 year time slices, from which the new tidal bathymetries were produced. These were then introduced into OTIS using the control settings in terms of friction.

Table 1. Changes in Dissipation[a]

Run Name	Shallow	Deep	Total
	M_2 Dissipation Change (GW)		
HT	4.8 (14.7)	−1.4 (−7.3)	3.5 (6.8)
HTE	9.4 (28.6)	0.7 (4.3)	10.2 (19.8)
No Ice	14.1 (43.0)	7.5 (40.8)	21.7 (42.2)
	K_1 Dissipation Change (GW)		
HT	−6.9 (−19.2)	−2.3 (−8.7)	−9.2 (−14.8)
HTE	−8.4 (−23.4)	−2.5 (−9.5)	−10.9 (−17.5)
No Ice	−9.0 (−25.2)	−2.5 (−9.5)	−11.5 (−18.6)

[a]Changes in M_2 and K_1 Dissipation rates (GW) compared to the control run for shallow water ($h < 1000$ m), deep ocean ($h > 1000$ m), and total (percent change in brackets).

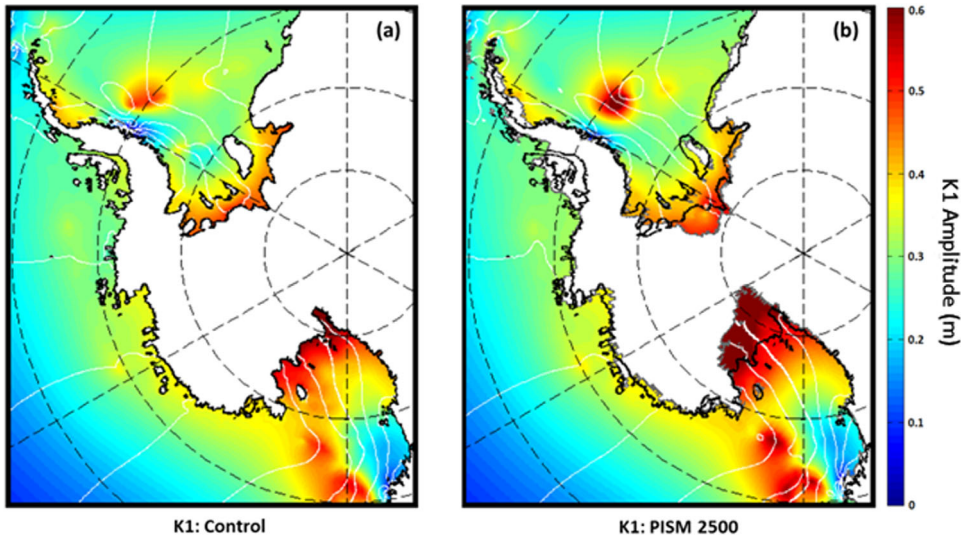

Figure 7. Comparison of K_1 amplitude resulting from ice anomalies output by the (b) ECP-8.5 scenario PISM-PIK run [data from *Winkelmann et al.*, 2012] (a) with the control run. The present day grounding line position is indicated by the thick black line and the new PISM-PIK grounding line in year 2500 is marked in gray in Figure 7b.

4.2. PISM-PIK Sensitivity Simulations

[17] The changes in ice sheet extent and thickness from the ECP run for PISM-PIK can be broadly divided into three tidally relevant parts: minor grounding line retreat along much of the Antarctic coastline, significant grounding line retreat along the Siple Ice Coast, and a partial collapse of the Ross Ice Shelf to a new, much reduced extent that appears to stabilize at around year 2350. Overall, the changes are focused around the Ross Sea area and this might explain why the modeled changes in the M_2 tidal constituent are very minor since the present day M_2 tide is very weak in this region. The changes in the Ross Sea, from year 2500 in the PISM-PIK model, result in considerable changes in the K_1 tidal constituent which are compared to the K_1 control run in Figure 7. While the general pattern of the tide remains the same, K_1 amplitudes across the entire region are generally increased by over 100%, leading to almost a 1m K_1 tidal amplitude along the Siple Ice Coast. K_1 amplitudes are also increased somewhat in the Weddell Sea, suggesting that the K_1 tidal constituent in this region is more sensitive to the position of the grounding line than the M_2 tide for this grounding line retreat scenario.

5. Discussion

[18] In this paper, we have undertaken studies of the sensitivity of M_2 and K_1 tides to the reduction in extent and thickness of Antarctic ice shelves. We are motivated by the known interactions between tides and ice shelves, and the possibility that these interactions may change in a warming world. Tidal response in amplitudes and dissipation rates are show in Table 2 to verify the resonance characteristics of the study areas for M_4, S_2, M_2, K_1, and O_1 tides. The results shown are horizontal averages of the amplitudes and dissipation from each area and chosen somewhat arbitrarily but such that the full response is covered. To further

Table 2. Horizontally Averaged Amplitudes (A) (m) and Dissipation Rates (D) (mW/m^2) From the Weddell and Ross Seas From the Resonance Analysis

	Period (h)									
	6.21		12		12.42		23.9		25.82	
Run	A	D	A	D	A	D	A	D	A	D
					Weddel Sea region					
Control	0.0191	0.0171	0.6907	6.5212	0.9565	13.2868	0.3566	0.7373	0.3511	0.6524
HT	0.8871	623.6119	0.5558	10.8296	0.8871	28.2164	0.3441	0.9127	0.3398	0.7812
HTE	0.9338	673.8912	0.5705	12.503	0.9338	34.0886	0.3392	0.9322	0.3337	0.7918
No Ice	0.968	917.6976	0.5755	17.3798	0.968	48.9239	0.3355	1.1181	0.3319	0.9708
					Ross Sea region					
Control	0.0029	0.0004	0.1355	1.437	0.0755	0.2402	0.392	1.8454	0.3175	0.9036
HT	0.0528	1.2323	0.0516	0.139	0.0527	0.1257	0.3768	1.7882	0.3078	0.9694
HTE	0.0566	1.405	0.0537	0.1632	0.0565	0.1572	0.3786	1.7792	0.3088	0.9596
No Ice	0.0666	3.4386	0.0595	0.1916	0.0665	0.2116	0.3702	1.7999	0.3032	1.0011

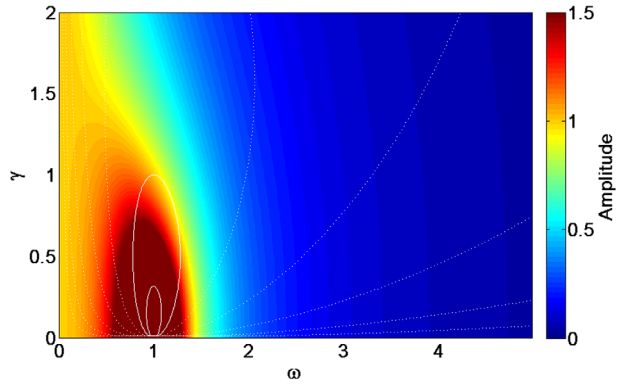

Figure 8. Amplitude (in color) and $\log_{10}$ dissipation (white lines) for a damped harmonic oscillator for different values of damping (γ) and forcing frequency (ω). Note that the units are arbitrary.

elucidate the mechanisms behind the results, we also look at the amplitudes and dissipation rates in a simple damped harmonic oscillator [see also *Egbert et al.*, 2004; *Arbic et al.*, 2009]. In its simplest form, we thus solve $\partial_{tt}u+\gamma\partial_t u+u=\sin(\omega t)$, where ω is the forcing frequency, γ is the damping coefficient, and subscripts denote derivation. It is easily shown that the amplitude of the oscillation is $A=1/\sqrt{(1-\omega^2)^2+(\gamma\omega)^2}$ and the dissipation comes out as $D=0.5\Re[i\omega/(1+i\gamma\omega-\omega^2)]$ (see Figure 8 for the results). Note that the solution in Figure 8 has arbitrary units, and rather than obtain a quantitative result for each of the ice shelves, the oscillator is introduced as a concept to provide qualitative arguments for why we see the responses we do in the simulations. Also note that our sensitivity runs effectively have a reduced damping because the ice is removed, leading to reduced frictional effects.

[19] In the Weddell Sea, the M_2 amphidromic point moves further off shelf as the ice shelf bathymetry changes, and there is consequently an increase in the tidal amplitude near the coast (Figure 2). However, the overall tidal amplitudes decrease in the Weddell Sea in the perturbation runs (Table 2), but the dissipation increases. This is because of an enhanced dissipation further off shelf in the Weddell Sea (near the shelf break; see Figure 1) which shifts the amphidromic point in the area and provides an enhanced amplitude closer to the coastline. In (nonresonant) tidal systems large enough to be influenced by rotation, amphidromic points will shift toward an area of increased dissipation [e.g., *Taylor*, 1921; *Pelling et al.*, 2013]. This is the picture we see here for M_2, with an enhanced tidal dissipation in the outer part of the Weddell Sea due to the removal of the ice shelves, and a shift outward of the amphidromic point (Figures 1 and 2).

[20] Table 2 also shows that the Weddell Sea becomes resonant for M_4 in the sensitivity runs. The decrease in semidiurnal amplitudes in the perturbation runs is associated with an increased dissipation rate, however, suggesting that the Weddell Sea experiences a shift in its natural frequency when the damping is reduced (see Figure 8; with only a reduced damping it is not possible in this setup to have both increased dissipation and a decreased amplitude). The real surprise lies in the quarter diurnal band, which has been neglected previously in the area because the (control) amplitudes are very small. In the sensitivity simulations, however, the M_4 tide becomes very energetic and is almost as large as the M_2 tide in the Weddell Sea. There is consequently a significantly enhanced dissipation of M_4 energy, which—since the damping is reduced in the sensitivity runs—must signify that the Weddell Sea has become resonant for the quarter diurnal period.

[21] The Ross Sea results (Table 2) show only minor changes for the longer period tides, again with a general decrease as part of the damping (i.e., the ice shelf) is reduced or removed. The exception is again in M_4, which is characterized by a very large increase in dissipation. The reason for this is most likely that the Ross Sea, like the Weddell Sea, becomes resonant for M_4 when the ice/damping is removed. The changes in dissipation between the control and sensitivity runs are also of interest, particularly since these could affect basal melt rates beneath the ice shelves. The increase in M_2 dissipation of up to 40% is due to the tide becoming more energetic as more ice shelf is removed. The dissipation is generally reduced beneath the Ronne-Filchner Ice Shelf but increases at the shelf edge of the Weddell Sea and around the tip of the Antarctic Peninsula. Changes in spatial distribution of dissipation do not necessarily match those in amplitude because the dissipation depends on the cube of velocity which in turn is controlled by water depth and the surface slope.

[22] The K_1 dissipation responds differently to the ice extent changes than does M_2: the K_1 tide decreases compared to the control run in our sensitivity runs. Here we see the areas of most reduction at the shelf break of the Ross and Weddell Seas, particularly along the western boundary where the tidal wave enters the embayment. Unlike the changes in M_2 dissipation, there is no notable change beneath either ice shelf and in fact almost all change is negative, typically around −20% over the entire domain, with no large regions of increased dissipation.

[23] Some caution should be used when interpreting these results since the present day model overestimates tidal amplitudes to some extent. We are not proposing a realistic future scenario but rather a sensitivity study; however, since the amplitudes in the perturbation runs are also most likely overestimated the difference between the two can still be considered a valid signal. Better parameterization of the ocean/ice shelf interaction in future studies, particularly in the hinging zone, since this is the main missing process in the region, along with higher resolution bathymetry, may go some way to improving this. It is also important to note that changes in tides resulting from altering ice shelf geometry are likely to be accompanied by changes in the exchange of water masses from the ice shelf cavity to the open ocean; this is not modeled here.

[24] Major thinning and/or retreat of ice from the Ronne-Filchner Ice Shelf is very likely to produce feedbacks arising from increased M_2 tidal amplitude. Since the pattern of changes are not all in the same direction these feedbacks may be positive or negative, but generally amplitudes are found to increase. Because of the nature of the relationships between tidal amplitudes and ice shelves and ice streams, these feedbacks are considered dominantly positive. The Ross Ice Shelf shows a similar response to the K_1 tide but only when grounding line retreat is included as in the tidal

runs arising from the PISM-PIK results. The asymmetry in surface velocities resulting from the nonlinear response to the inclusion of tides in the ice stream model presented by *Gudmundsson* [2011] leads to increases in mean velocity of about 5%. Extrapolating these results to estimate the effect of the increase in tides on ice stream velocities is not trivial due to the nonlinearity inherent in this relationship. While the impacts of the changes in M_2 and K_1 amplitudes on ice shelf or ice sheet dynamics are not modeled directly here, a doubling of tidal amplitude under the Ronne-Filchner Ice Shelf cannot be ignored as a feedback on both ice shelf stability and ice stream velocity. The ice streams draining the WAIS sector of the Ronne-Filchner Ice Shelf would appear to be particularly vulnerable, including the Evans, Carlson, Rutford, Institute, Foundation, and Support-Force systems [*Rignot and Thomas*, 2002]. In addition, the changes in dissipation calculated for our sensitivity simulations suggest that this is another important factor to consider when evaluating the effects on ice dynamics through changes in basal melting. There is therefore a requirement to investigate both the impact of tidal motion on calving and ice stream processes and rates, and to couple ice sheet models with tidal models to further constrain this hitherto neglected Earth system feedback that has potentially significant implications for our understanding of past and possible future major ice sheet collapse.

[25] **Acknowledgments.** Funding was provided by the Natural Environmental Research Council through grants NE/J/500203/1 (SHRR PhD studentship) and NE/F/014821/1 (JAMG Advanced Fellowship). J.A.M.G. and J.D.S. acknowledge funding from the Climate Change Consortium of Wales (C3W), and R.W. received support from the German Federal Ministry of Education and Research (BMBF grant 01LP1171A). Comments from Paul Holland and three anonymous reviewers greatly improved the manuscript.

References

Aethalgeirsdottir, G., A. M. Smith, T. Murray, M. A. King, K. Makinson, K. W. Nicholls, and A. E. Behar (2008), Tidal influence on Rutford Ice Stream, West Antarctica: Observations of surface flow and basal processes from closely spaced GPS and passive seismic stations, *J. Glaciol.*, *54*, 715–724.

Anandakrishnan, S., D. E. Voigt, R. B. Alley, and M. A. King (2003), Ice stream D flow speed is strongly modulated by the tide beneath the Ross Ice Shelf, *Geophys. Res. Lett.*, *30*(7), 1361, doi:10.1029/2002GL016329.

Arbic, B. K., S. T. Garner, R. W. Hallberg, and H. L. Simmons (2004a), The accuracy of surface elevations in forward global barotropic and baroclinic tide models, *Deep Sea Res., Part II*, *51*, 3069–3101.

Arbic, B. K., D. R. MacAyeal, J. X. Mitrovica, and G. A. Milne (2004b), Palaeoclimate—Ocean tides and Heinrich events, *Nature*, *432*, 460.

Arbic, B. K., R. H. Karsten, and C. Garrett (2009), On tidal resonance in the global ocean and the back-effect of coastal tides upon open-ocean tides, *Atmos. Ocean*, *47*, 239–266.

Bamber, J. L., R. B. Alley, and I. Joughin (2007), Rapid response of modern day ice sheets to external forcing, *Earth Planet. Sci. Lett.*, *257*, 1–13.

Bindschadler, R. A., M. A. King, R. B. Alley, S. Anandakrishnan, and L. Padman (2003), Tidally controlled stick-slip discharge of a West Antarctic Ice Stream, *Science*, *301*, 1087–1089.

Conway, H., B. L. Hall, G. H. Denton, A. M. Gades, and E. D. Waddington (1999), Past and future grounding-line retreat of the West Antarctic Ice Sheet, *Science*, *286*, 280–283.

Egbert, G. D., and S. Y. Erofeeva (2002), Efficient Ocean modeling of barotropic ocean tides, *J. Atmos. Oceanic Technol.*, *19*, 183–204.

Egbert, G. D., and R. D. Ray (2001), Estimates of M2 tidal energy dissipation from Topex/Poseidon altimeter data, *J. Geophys. Res.*, *106*, 22,475–22,502.

Egbert, G. D., R. D. Ray, and B. G. Bills (2004), Numerical modeling of the global semidiurnal tide in the present day and in the Last Glacial Maximum, *J. Geophys. Res.*, *109*, C03003, doi:10.1029/2003JC001973.

Fluckiger, J., R. Knutti, and J. W. C. White (2006), Oceanic processes as potential trigger and amplifying mechanisms for Heinrich Events, *Paleoceanography*, *21*, PA2014, doi:10.1029/2005PA001204.

Glasser, N. F., and T. A. Scambos (2008), A structural glaciological analysis of the 2002 Larsen B ice shelf collapse, *J. Glaciol.*, *54*, 3–16.

Goldberg, D., D. M. Holland, and C. Schoof (2009), Grounding line movement and ice shelf buttressing in marine ice sheets, *J. Geophys. Res.*, *114*, F04026, doi:10.1029/2008JF001227.

Green, J. A. M. (2010), Ocean tides and resonance, *Ocean Dyn.*, *60*, 1243–1253.

Green, J. A. M., and M. Huber (2013), Tidal dissipation in the early Eocene and implications for ocean mixing, *Geophys. Res. Lett.*, *40*, 2707–2713, doi:10.1002/grl.50510.

Green, J. A. M., and J. Nycander (2013), A comparison of internal wave-drag parameterizations for tidal models, *J. Phys. Ocean.*, *43*, 104–119.

Griffiths, S. D., and R. W. Peltier (2009), Modeling of polar ocean tides at the last glacial maximum: Amplification, sensitivity and climatological implications, *J. Clim.*, *22*, 2905–2924.

Gudmundsson, G. H. (2011), Ice-stream response to ocean tides and the form of the basal sliding law, *Cryosphere*, *5*, 259–270, doi:10.5194/tc-5-259-2011.

Hellmer, H. H., F. Kauker, R. Timmermann, J. Determann, and J. Rae (2012), Twenty-first-century warming of a large Antarctic ice-shelf cavity by a redirected coastal current, *Nature*, *485*, 225–228, doi:10.1038/nature11064.

Hemming, S. R. (2004), Heinrich events: Massive late Pleistocene detritus layers of the North Atlantic and their global climate imprint, *Rev. Geophys.*, *42*, RG1005, doi:10.1029/2003RG000128.

King, M. A., T. Murray, and A. M. Smith (2010), Non-linear responses of Rutford Ice Stream, Antarctica, to semi-diurnal and diurnal tidal forcing, *J. Glaciol.*, *195*, 167–176.

King, M. A., K. Makinson, and G. H. Gudmundsson (2011), Nonlinear interaction between ocean tides and the Larsen C Ice Shelf system, *Geophys. Res. Lett.*, *38*, L08501, doi:10.1029/2011GL046680.

Lythe, M. B., and D. G. Vaughan (2001), BEDMAP: A new ice thickness and subglacial topographic model of Antarctica, *J. Geophys. Res.*, *106*, 335–351.

MacAyeal, D. R. (1984), Numerical simulations of the Ross Sea tides, *J. Geophys. Res.*, *89*, 607–615.

Makinson, K., P. R. Holland, A. Jenkins, K. W. Nicholls, and D. M. Holland (2011), Influence of tides on melting and freezing beneath Filchner-Ronne Ice Shelf, Antarctica, *Geophys. Res. Lett.*, *38*, L06601, doi:10.1029/2010GL046462.

Martin, M. A., R. Winkelmann, M. Haseloff, T. Albrecht, E. Bueler, C. Khroulev, and A. Levermann (2011), The Potsdam Parallel Ice Sheet Model (PISM-PIK), Part II: Dynamical equilibrium simulation of the Antarctic Ice Sheet, *Cryosphere*, *5*, 727–740.

Meinshausen, M., et al. (2011), The RCP greenhouse gas concentrations and their extensions from 1765 to 2300, *Clim. Change*, *109*, 213–241.

Mueller, R. D., L. Padman, M. S. Dinniman, S. Y. Erofeeva, H. A. Fricker, and M. A. King (2012), Impact of tide-topography interactions on basal melting of Larsen C Ice Shelf, Antarctica, *J. Geophys. Res.*, *117*, C05005, doi:10.1029/2011JCO07263.

Ó Cofaigh, C. (2011), Past ice-shelf collapse in West Antarctica, *Nature*, *476*, 290–291.

Padman, L., and H. A. Fricker (2005), Tides on the Ross Ice Shelf observed with ICESat, *Geophys. Res. Lett.*, *32*, L14503, doi:10.1029/2005GL023214.

Padman, L., S. Y. Erofeeva, and H. A. Fricker (2008), Improving Antarctic tide models by assimilation of ICESat laser altimetry over ice shelves, *Geophys. Res. Lett.*, *35*, L22504, doi:10.1029/2008GL035592.

Padman, L., H. A. Fricker, R. Coleman, S. Howard, and L. Erofeeva (2002), A new tide model for the Antarctic ice shelves and seas, *Ann. Glaciol.*, *34*, 247–254.

Pelling, H. E., and J. A. M. Green (2013), Sea-level rise, tidal power, and tides in the Bay of Fundy, *J. Geophys. Res.*, *118*, 1–11, doi:10.1002/jgrc.20221.

Pelling, H. E., J. A. M. Green, and S. L. Ward (2013), Tides and sea-level rise: to flood or not to flood, *Ocean Modell.*, *60*, 21–29.

Pritchard, H. D., S. R. M. Ligtenberg, H. Fricker, D. G. Vaughan, M. R. van den Broeke, and L. Padman (2012), Antarctic ice-sheet loss driven by basal melting of ice shelves, *Nature*, *484*, 502–505.

Rignot, E., and R. H. Thomas (2002), Mass balance of polar ice sheets, *Science*, *297*, 1502–1506.

Rignot, E., G. Casassa, P. Gogineni, W. Krabill, A. Rivera, and R. Thomas (2004), Accelerated ice discharge from the Antarctic Peninsula following the collapse of Larsen B ice shelf, *Geophys. Res. Lett.*, *31*, L18401, doi:10.1029/2004GL020697.

Rott, H., F. Müller, T. Nagler, and D. Floricioiu (2011), The imbalance of glaciers after disintegration of Larsen-B ice shelf, Antarctic Peninsula, *Cryosphere*, *5*, 125–134.

Schoof, C. (2007) Ice sheet grounding line dynamics: Steady states, stability, and hysteresis, *J. Geophys. Res.*, *112*, F03S28, doi:10.1029/2006JF000664.

Shepherd, A., D. Wingham, D. Wallis, K. Giles, S. Laxon, and A. V. Sundal (2010), Recent loss of floating ice and the consequent sea level contribution, *Geophys. Res. Lett.*, *37*, L13503, doi:10.1029:2010GL042496.

Taylor, G. (1921), Tidal oscillations in gulfs and rectangular basins, *Proc. London Math. Soc.*, *20*, 148–181.

Vieli, A., and F. M. Nick (2011), Understanding and modeling rapid dynamic changes of tidewater outlet glaciers: Issues and implications, *Surv. Geophys.*, *32*, 437–458.

Winberry, J., S. Anandakrishnan, R. Alley, R. A. Bindschadler, and M. A. King (2009), Basal mechanics of ice streams: Insights from the stick-slip motion of Whillans Ice Stream, West Antarctica, *J. Geophys. Res.*, *114*, F01016, doi:10.1029/2008JF001035.

Winkelmann, R., M. A. Martin, M. Haseloff, T. Albrecht, E. Bueler, C. Khroulev, and A. Levermann (2011), The Potsdam parallel Ice Sheet Model (PISM-PIK), Part I: Model description, *Cryosphere*, *5*, 715–726.

Winkelmann, R., A. Levermann, K. Frieler, and M. A. Martin (2012), Uncertainty in future solid ice discharge from Antarctica, *Cryosphere Discuss.*, *6*, 673–714.

Zaron, E., and G. Egbert (2006), Estimating open-ocean barotropic tidal dissipation: The Hawaiian Ridge, *J. Phys. Ocenaogr.*, *36*, 1019–1035.